

Colloidal ionic complexes on periodic substrates: Ground-state configurations and pattern switching

Samir El Shawish

Department of Theoretical Physics, Jozef Stefan Institute, Jamova 39, 1000 Ljubljana, Slovenia

Jure Dobnikar

*Department of Chemistry, University of Cambridge, Lensfield Road, CB2 1EW Cambridge, United Kingdom**Department of Theoretical Physics, Jozef Stefan Institute, Jamova 39, 1000 Ljubljana, Slovenia*

Emmanuel Trizac

Université Paris–Sud, Laboratoire de Physique Théorique et Modèles Statistiques (CNRS UMR 8626), F-91405 Orsay Cedex, France

(Received 20 September 2010; revised manuscript received 17 December 2010; published 11 April 2011)

We theoretically and numerically studied ordering of “colloidal ionic clusters” on periodic substrate potentials such as those generated by optical trapping. Each cluster consists of three charged spherical colloids: two negatively and one positively charged. The substrate is a square or rectangular array of traps, each confining one such cluster. By varying the lattice constant from large to small, the observed clusters are first rodlike and form ferro- and antiferrolike phases, then they bend into a bananalike shape, and finally they condense into a percolated structure. Remarkably, in a broad parameter range between single-cluster and percolated structures, we have found stable supercomplexes composed of six colloids forming grapelike or rocketlike structures. We investigated the possibility of macroscopic pattern switching by applying external electrical fields.

DOI: [10.1103/PhysRevE.83.041403](https://doi.org/10.1103/PhysRevE.83.041403)

PACS number(s): 82.70.Dd, 41.20.Cv, 79.60.Jv, 82.70.Kj

I. INTRODUCTION

It is generally considered that the study of colloidal systems started with the work of Thomas Graham, around 1860, although substances such as the “purple of Cassius,” which turns out to be colloidal gold, were used by glassmakers and porcelain manufacturers as early as the 17th century [1]. For a long period, those systems were considered as “unmanageable” (see, e.g., the preface of Ref. [1]), due, in particular, to the difficulty to characterize them precisely (size, shape, charge, etc.) and also to the lack of theoretical tools to understand effective interactions. From this perspective, a decisive step forward occurred in the 1940s with the work of Derjaguin, Landau, Verwey, and Overbeek [2], which helped turn the initial empiricism into a more solid body of knowledge. More recently, progress in experimental manipulation techniques promoted colloids as interesting model systems to investigate a large gamut of fundamental physical phenomena: phase ordering, nucleation, effects of confinement and reduced dimensionality, interfacial phenomena, and various nonequilibrium problems including glass formation, to name but a few. Indeed, compared to atomic systems, colloids offer four advantages: first, they are characterized by small elastic constants and therefore they are easy to manipulate (“soft matter”); second, they are more easily visualized since their typical length scale is within the range of visible light; third, the corresponding time scale is no longer in the picosecond range, but of order 1 s; fourth, their effective interaction potential may be easily tuned to some extent by changing some control parameter such as the concentration of a given solute [3]. Such features stem, directly or indirectly, from the large size (on an atomic scale) of the mesoscopic constituents. Hence, colloids can be considered as “big atoms” [4], but with controllable interactions, and it is noteworthy that they may furthermore exhibit new structures that do not seem to have any atomic analog [5].

Of particular interest here is a class of charged colloidal spheres in the presence of optical trap arrays, where a wide variety of crystalline states has been reported [6–12]. On a two-dimensional modulated substrate, multiple charged colloids can be confined in sufficiently strong traps, and thereby form n -mers that exhibit an orientational degree of freedom. It has been established from experimental, numerical, and theoretical approaches [6–12] that such systems may show remarkably rich orientational ordering and lead to the formation of so called colloidal molecular crystals.

Previous approaches considered situations in which the colloids forming trapped n -mers are like-charged objects. On the other hand, the “molecules” under study here are made up of oppositely charged colloids, with equal charges in absolute value. The focus will be on a square lattice of traps, including also distorted geometries where all distances along one of the principal axes of the square are scaled by a given factor α , thereby producing a rectangular lattice. We will restrict our attention to the ground state, leaving thermal effects for further studies [13]. Under these circumstances, it has been shown that in the dipolar case (with trapped clusters each formed of two oppositely charged colloids) the resulting orientational behavior is somehow trivial: the observed phase is made up of $ABAB$ -type stripes, where the dipoles in stripe A are aligned along the stripe (up) while those in stripe B have opposite orientation [12]. Furthermore, the stripe structure cannot be tuned by modifying the lattice constant or salt content in the solution. Here we consequently consider clusters with three colloids, two negatively and one positively charged, which are more amenable to an external control, and display a wealth of ordering patterns, which is the focus of our interest. The paper is organized as follows. The model and the methods are defined in Sec. II, where the differences in modeling with previous works are outlined. The behavior on square and rectangular lattices with an isotropic parabolic confinement potential is

studied in Sec. III, and in Sec. IV we discuss the relevance of these results in the case of a more realistic cosine trap potential. All these results pertain to equilibrium configurations, while orientational pattern modifications induced by an external electric field are finally addressed in Sec. V. In the conclusion, we summarize our main findings and discuss perspectives and unresolved problems.

II. MODEL AND METHODS

We consider a mixture of negatively and positively spherical and homogeneously charged colloids, with stoichiometry 2:1 (twice as many negative than positive macroions, which is equivalent to the situation in which all charges are reversed). Those mesoscopic objects bear a total charge that is neutralized by an ensemble of microions. We assume that counterions and electrolyte microions do not differ. The colloids are confined in a two-dimensional (2D) plane by the action of laser beams. This plane is furthermore corrugated by additional preferential confinement: the colloids, subject to gradient forces and light pressure [6,14], tend to gather in the regions of highest laser intensity. It is then experimentally possible to create a 2D periodic substrate of traps, with variable geometry. It should be emphasized that the microions are not sensitive to confinement, so that our 2D colloidal system is immersed in a standard electrolyte that mediates between the charged colloids a screened Coulomb interaction of the form [2,15,16]

$$V_C = K \sum_{j \neq i} s_{ij} \frac{e^{-\kappa r_{ij}}}{r_{ij}/l}. \quad (1)$$

The energy scale K , which contains a geometric prefactor together with the squared effective charge of the colloids [17], is not relevant for our purposes, since we are interested in ground-state configurations. In Eq. (1), the sum runs over all colloidal pairs with interaction sign $s_{ij} = \pm 1$ distinguishing like from oppositely charged colloids, and interparticle distance r_{ij} between macroions i and j ; with l we denote the intertrap distance, see Fig. 1. We therefore implicitly assumed that oppositely charged colloids at contact also interact through a screened Coulomb form, whereas such a

functional dependence is better suited to describe the far-field behavior [18]. We note, however, that as long as we are comparing phases with an equal number of doublet $+ -$ at contact, such configurations contribute a constant to the total energy, so that considering more exact forms of interaction potential at short scale would not alter our conclusions. In Eq. (1), $1/\kappa$ denotes the Debye length, which can be tuned changing the electrolyte density. Strictly speaking, Eq. (1) is not an energy but a free energy, since it includes an entropic contribution from the microions [19].

In addition to interparticle forces (two-body and pairwise additive), the colloids feel an external (one-body) potential due to laser modulation, and it is the subtle interplay between both kinds of forces that selects the type of ionic complexes that are formed in each trap and their relative arrangement from trap to trap. In [8,9], it was assumed that the colloidal complexes in a given trap (dimers, trimers, etc.) form a rigid object, with a single orientational degree of freedom, which effectively allows us to omit the laser-induced potential in the analysis. The situation with oppositely charged colloids, however, differs: take an isolated triplet $- + -$ in the aligned geometry that minimizes its self-energy. Such an object invariably bends under strong confinement, thereby forming a “bananalike” object. The shape of the banana depends on the parameters (salinity, intertrap distance, etc.), and should be determined self-consistently. We therefore do not lump substrate potential effects into a unique quantity as in [8,9], but explicitly consider each colloidal degree of freedom in the analysis. This rules out the discrete angle approach invoked in [9], where only a restricted set of possible orientations was considered. We also note that already at the level of like-charged colloids, our recent work [10] evidenced some subtle shortcomings of the rigid n -mer approach.

The system obviously bears some resemblance to the molecules on the atomic scale. However, in our model the binding is the result of the attractive Yukawa interactions and the confinement potentials and is therefore relatively weak compared to the strong covalent bonds typical in real molecules. We have consequently chosen to call the n -meric colloidal structures “clusters” or “complexes” rather than “molecules” as has been done elsewhere (see [7–10]). In spirit, our study then belongs to a more general line of research pertaining to colloidal clusters [20]. The previous references, however, generally deal with large assemblies, whereas our clusters are made up of a small number of colloids.

In all our considerations, the ratio of the total number of colloids to the total number of traps is exactly three, therefore under strong enough confinement, there are exactly three colloids per trap and the ground state is paved with trimers ($- + -$) of varying shapes and orientations. These mesoscopic objects bear a net charge, which is neutralized by microions in solution. It has been realized [8,10] that it is not necessary to invoke local anisotropies of the confinement potential to account for the observed ground states: there is an obvious source of anisotropy in the lattice geometry itself; however, in the vicinity of a trap minimum, the confined particles feel an isotropic (2D) potential. In this case, the screened Coulomb potential alone is able to select preferred orientations for the clusters (whereas as alluded to above, the effective spin

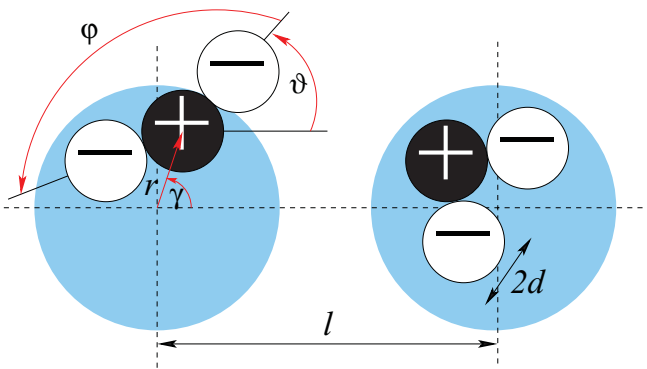


FIG. 1. (Color online) Sketch of two clusters—each made up of three colloids—in two different potential traps, with definition of the relevant quantities. The center of a blue area denotes the confining potential minimum and l is therefore the intertrap distance. The same color code will be used throughout the rest of the paper: black (white) dots for positively (negatively) charged colloids.

model considered in [9] restricted possible orientations to the principal directions of the light lattice). Here we wish to avoid introducing an orientational bias through the trap potential, and therefore initially consider the parabolic confinement. The total dimensionless energy of colloid i reads

$$e_i = A(\delta_i/l)^2 + \sum_{j \neq i} s_{ij} \frac{e^{-\kappa r_{ij}}}{r_{ij}/l}, \quad (2)$$

where δ_i denotes the distance between the colloid i center of mass and the center of the trap to which it belongs, and A measures the relative importance of parabolic confinement over Coulombic forces. Each triplet of colloids belongs to a “native” trap, so the colloids are not allowed to hop from one trap to another. Such a limitation precludes the sliding states studied in [21] under the influence of an external electric field. We note that the experimental situation is somehow intermediate between the point of view adopted here—*a priori* mostly relevant for strong confinement conditions—and that used in [9], see the discussion in [10]. For completeness, we have also performed simulations with a “realistic” potential in the spirit of [7] to assess the validity of the isotropic approach.

At constant temperature, three parameters govern the behavior of the system: the relative magnitude of the confinement with respect to the Yukawa interaction A , the ratio of the colloid radius to the Debye screening length κd , and the ratio of the lattice spacing to Debye length κl . In the rectangular case, the lattice aspect ratio α should be included. A trimer in two dimensions has six degrees of freedom, but only four of them are independent assuming the colloids are in contact. The arrangement of colloids in the vicinity of a trap center can therefore be described by four quantities (see Fig. 1): the position of the cluster’s center of mass relative to the trap minimum is described by r and γ , the relative orientation of its axis with respect to a fixed direction (say a line joining the centers of two neighboring traps) by the angle ϑ , and the amount of bending by ϕ ($\phi = \pi$ for rodlike and $\phi < \pi$ for bent structures).

Ground-state configurations were obtained by the energy minimization (EM) technique and tested by standard Monte Carlo (MC) annealing simulations. To reduce the number of minimizing parameters in EM, an assumption on the ground-state structure was preset. For a given rectangular lattice, we decided to partition the lattice to two (A - B) or four (A - B - C - D) sublattices, which in general form a checkerboard or a stripe (chain) pattern. Since each colloidal cluster is parametrized by four quantities (see Fig. 1), a p -partite ($p = 2, 4$) assumption in EM would correspond to $4p$ minimizing parameters. We used standard numerical routines (simplex and quasi-Newton algorithm [22]) for finding the (local) minimum; by repeating the EM procedure several ($\sim 10^4$) times over $4p$ different initial estimates, we eventually converged to a global minimum. However, in extreme parameter regimes (i.e., $l/d \gg 1$ or close to phase transitions), the convergence became slower due to many almost degenerate local minima and the ground state was identified among selected candidates—by directly comparing their energies.

The 2- and 4-partite constraint used in EM was further assessed by standard MC annealing simulations. We checked all interesting regions of the phase diagram by running several

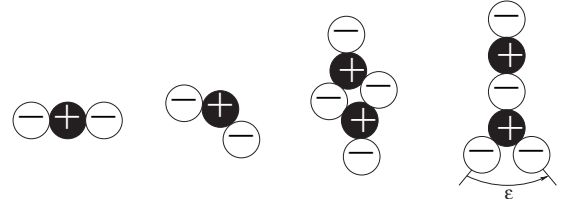


FIG. 2. Summary of the most frequent composite clusters encountered in our study (from left to right): straight trimer, banana \mathcal{B} , grape \mathcal{G} , rocket \mathcal{R} .

MC simulations starting from different initial configurations (both minimal or close-to-minimal EM structures and random configurations) and used the annealing method with an exponentially decaying temperature profile. We tried several system sizes with 2×2 , 4×4 , and 16×16 traps using periodic boundary conditions. As a result, we identified and confirmed all shapes obtained in EM. However, due to the tiny energy differences and large energy barriers between local minima, long relaxation times (i.e., 10^8 MC steps for a 4×4 system array) were needed to obtain exactly the same orientational orders as in EM. Hence, the system easily gets trapped at low annealing temperature in some local metastable phase composed of domains of various ground-state patterns [23].

III. SQUARE AND RECTANGULAR LATTICE CONFINEMENT

Before embarking on a detailed study, we first give an overview (Fig. 2) of the various composite objects that we have observed in our simulations. When the traps were well separated, we observed isolated trimers, either straight or banana-shaped \mathcal{B} . For very small trap separation l , percolated chainlike structures \mathcal{C} rather than clusters are stable. In the intermediate region, “superclusters” composed of six colloids appear. They are formed by two neighboring trimers forming the supercluster by minimizing their total energy (paying the penalty due to the confinement while reducing the electrostatic interaction energy) [24]. We observed two typical shapes and coined them grape \mathcal{G} and rocket \mathcal{R} . In Fig. 3, we further provide a summary of different orientational orderings and propose a nomenclature to classify them.

A. Square lattices

Figures 4 and 5 show the type of orderings that occur on a square lattice ($\alpha = 1$) at two different pinning amplitudes

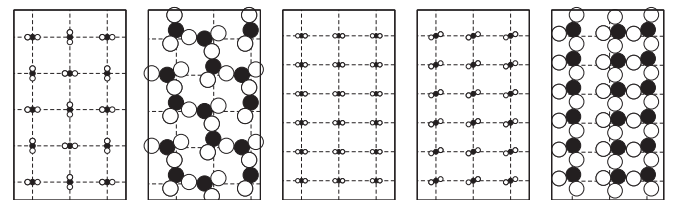


FIG. 3. Sketch of the different ordering patterns that will be reported (from left to right): antiferro \mathcal{A} , chain \mathcal{C} , ferro \mathcal{F} , tilted ferro \mathcal{F}^* , and ladder \mathcal{L} . Dashed lines represent a square (or rectangular) lattice of traps.

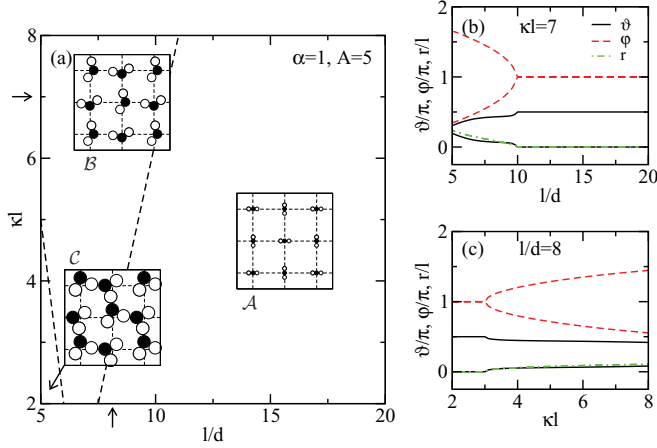


FIG. 4. (Color online) (a) Ground-state phase diagram at a relatively strong substrate potential ($A = 5$) for colloidal trimers on a square lattice. Typical snapshot configurations are calculated using $(l/d, \kappa l) = (7, 2)$ for the B phase, $(15, 4)$ for the A structure, and $(5, 2)$ for the C phase. The lines between the different phases are shown as a guide to the eye. (b) Values of the three quantities characterizing the cluster shape [red dashed (upper), r ; black solid, ϑ ; and green dot-dashed (lower), ϕ] as a function of the ratio l/d at constant $\kappa l = 7$. (c) Values of the same three quantities as a function of κl at constant $l/d = 8$.

(embodied in the parameter A). In panel (a) we show the phase diagram separating the regions of stability of phases and the corresponding snapshots of the typical cluster arrangements. Panels (b) and (c) display the variation of three quantities characterizing the cluster shape and their orientational ordering. The transitions from straight to bent shapes are clearly seen on bifurcating red curves. It should be stressed that ϕ and $2\pi - \phi$ represent the same shape, and the two branches do not indicate two different structures. The black curves showing the cluster orientation have two branches with ϑ_1 and ϑ_2 . The special case is the A (antiferro) phase, where $(\vartheta_1, \vartheta_2) = (0, \pi/2)$. For straight clusters, the angles ϑ and $2\pi - \vartheta$ are equivalent, but this is no longer true if they are bent. Therefore, the region with

four distinct branches in Fig. 5 represents a 4-partite structure with $\vartheta_1, \dots, \vartheta_4$. The values of r (green curves) tell us whether the clusters are displaced from the trap minima ($r \neq 0$) or not ($r = 0$). The values of the fourth defining quantity γ proved rather uninformative and were not included in the figures for clarity reasons.

At the stronger confinement (Fig. 4) we found three phases: isolated triplets in the antiferrolike arrangement A , bent (banana) triplets B whose angular arrangement varies continuously to antiferro A upon increasing l/d , and a percolated chain pattern (C) at very low l/d and small screening [lower left corner of Fig. 4(a)]. At weaker confinement (Fig. 5), two additional phases appear: rocket R and grape G , which are both nonpercolating and made up of the repetition of two-triplet (six colloids) objects.

In Fig. 4, all ground-state configurations have a 2-partite lattice structure, which has also been confirmed by the unconstrained MC annealing simulations. In the limit of small macroions, $l/d \gg 1$, we find stable isolated triplet configurations with quasidegenerate orientational preferences. For example, the antiferro A phase is slightly more favorable compared to the tilted ferro \mathcal{F}^* phase: at the $(l/d, \kappa l) = (15, 4)$ point in the phase diagram, the corresponding energies are $E_A/K = -2.4250$ and $E_{\mathcal{F}^*}/K = -2.4247$.

In Fig. 5, there are regions in the phase diagram where the 4-partite configurations appear to be favored over bipartite. The energy difference between 2- and 4-partite ordering, however, is extremely small. For example, in the representative rocket R and grape G phases shown in Fig. 5(a), the energies are, respectively, $E_{4p}/K = -0.5888$, $E_{2p}/K = -0.5870$, $E_{4p}/K = -2.723145$, and $E_{2p}/K = -2.723143$. Such small differences, $E_{4p} - E_{2p}$, imply that these ground-state configurations become unstable at small but finite temperatures and the formation of domains is expected in experiments and simulations. A similar effect is expected also for the A ground state, which should interfere with the nearest (in energy) \mathcal{F}^* phase, as in the previous $A = 5$ case in Fig. 5. On the other hand, the grape G phase in the $l/d \gg 1$ limit is well separated from the competing A phase ($E_A/K = -2.645310$ for the same κl and κd values).

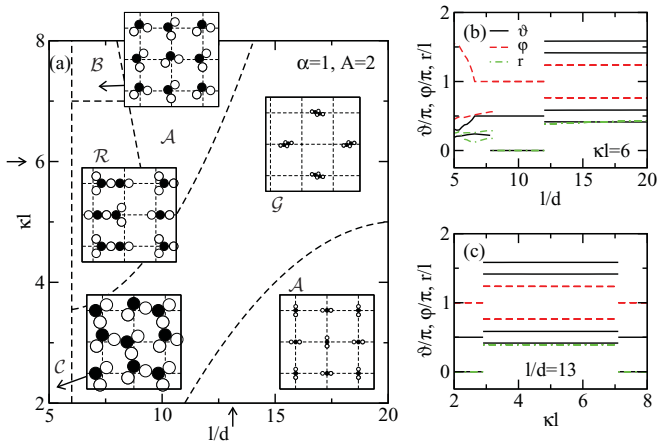


FIG. 5. (Color online) Same as Fig. 4 but for a relatively weak substrate potential ($A = 2$). Typical snapshot configurations are calculated using $(l/d, \kappa l) = (7, 8)$ for B , $(7, 4)$ for R , $(5, 2)$ for C , $(20, 8)$ for G , and $(15, 2)$ for A phase.

1. Antiferrolike phase

The occurrence of the A phase on the right-hand side of Figs. 4 and 5 can be rationalized along similar lines to what was done in Ref. [8]. For large enough values of κl and even larger l/d , it is legitimate to restrict the summation in Eq. (2) to nearest-neighbor traps (see [10] for a more complete discussion). It is also legitimate to assume that triplets align in straight configurations. The question is, therefore, to understand the relative orientation of triplets from trap to trap. Elaborating on the remark put forward in [25,26] that a nonisotropic charge distribution in an electrolyte creates an electric potential that is anisotropic at all scales and that does not have any simple “multipolar” symmetry, we write the angular dependence of the far-field potential of a triplet as [8]

$$V_{\text{tr}} = 2 \cosh(2\kappa d \sin \psi) - 1, \quad (3)$$

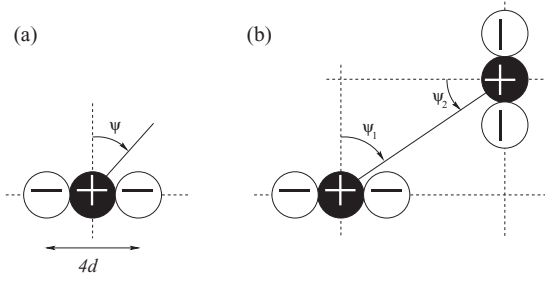


FIG. 6. Definition of the notations used to compute triplet-triplet interaction in the (aligned) straight case.

where the direction ψ is defined in Fig. 6(a). Consequently, the relevant angular-dependent triplet-triplet interaction potential may be written [see Fig. 6(b)]

$$V_{\text{tr/tr}} = [2 \cosh(2\kappa d \sin \psi_1) - 1][2 \cosh(2\kappa d \sin \psi_2) - 1]. \quad (4)$$

On a square lattice, and assuming bipartite structure (which is backed up by simulations), we then have to consider triplet-triplet interactions along both principal axes of the lattice. This leads to the following energy:

$$[2 \cosh(2\kappa d \sin \psi_1) - 1][2 \cosh(2\kappa d \sin \psi_2) - 1] + [2 \cosh(2\kappa d \cos \psi_1) - 1][2 \cosh(2\kappa d \cos \psi_2) - 1]. \quad (5)$$

The minimum is reached for $(\psi_1, \psi_2) = (0, \pi/2)$, irrespective of κd , which coincides exactly with the \mathcal{A} phase configuration. The situation changes on a rectangular lattice, see below. On the other hand, the $\mathcal{A} \rightarrow \mathcal{B}$ transition line observed in Fig. 4 can be explained as a one-cluster effect: in the absence of confinement, the trimers take on the straight shape due to the repulsion between the two positively charged colloids. However, by increasing the confinement or because of enhanced screening, the relative importance of the electrostatic repulsion decreases. We expect that for A and d fixed, there exists a critical inverse screening length κ^* beyond which the straight trimer bends (and ultimately forms an equilateral triangle if κ is very large). Since it is a one-triplet instability, κ^* should be independent of lattice spacing l , which translates into a straight line with slope $\kappa^* d$ in a $(\kappa l, l/d)$ plot such as Fig. 4(a). This corroborates our numerical finding with a straight separatrix between \mathcal{A} and \mathcal{B} phases. For $A = 2$, the argument does not hold since no transition from straight to bent shapes takes place.

2. Grape phase

The stability of the grape phase \mathcal{G} can be rationalized by comparing the self-energy per colloid

$$E_{\text{self}} = \frac{d}{6} \sum_{j \neq i=1}^6 s_{ij} \frac{e^{-\kappa r_{ij}}}{r_{ij}} \quad (6)$$

of different composite complexes in the absence of any trap potential. In Fig. 7, we have compared the self-energies of the following six-colloid objects: grape, rocket (with various angles ϵ , as defined in Fig. 2), and two distant trimers. Among these, the two distant trimers are the most stable in the bare Coulomb limit ($\kappa \rightarrow 0$) with $E_{\text{self}} \rightarrow -1/4$. However, as

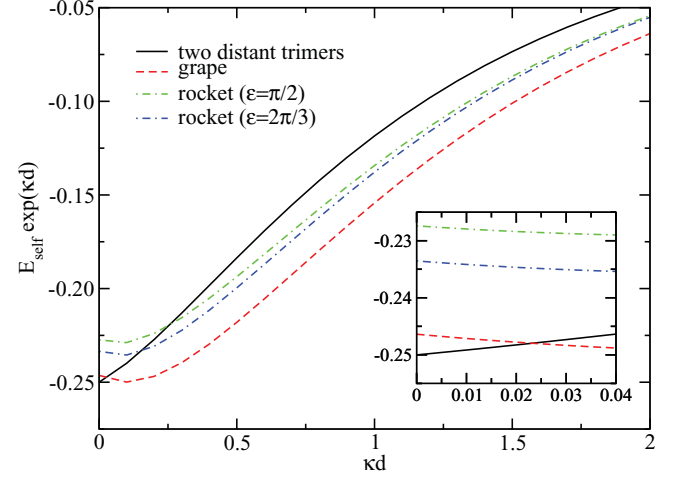


FIG. 7. (Color online) Coulombic self-energy of six colloids (two positively and four negatively charged) forming various complexes.

soon as $\kappa d > 2.2 \times 10^{-2}$, a fairly small number, the grape geometry is found to be the optimal one. Therefore, in almost the entire range of relevant values, the grape is energetically the most stable isolated object consisting of six colloids. Of course, on a corrugated substrate, the confining potential influences the above scenario by penalizing extended structures, and the intercluster interaction affects the picture as well, however there is still a substantial region in Figs. 5 and 8 (see below) where the grape phase remains stable.

B. Rectangular lattice of traps

Distorting lattice geometry by changing the aspect ratio away from the square shape ($\alpha \equiv l_y/l_x < 1$) induces new orderings to the list of ground-state configurations reported above. Figure 8 shows ground-state phase diagrams for $\alpha = 0.8$ and two pinning potentials, where three new phases emerge with respect to the square ($\alpha = 1$) case: a ferro \mathcal{F} phase and a tilted ferro \mathcal{F}^* phase, which evolves into a familiar banana \mathcal{B} phase at smaller l/d and $A = 5$, and a percolating ladder \mathcal{L} phase in a weaker confinement ($A = 2$). The latter consists

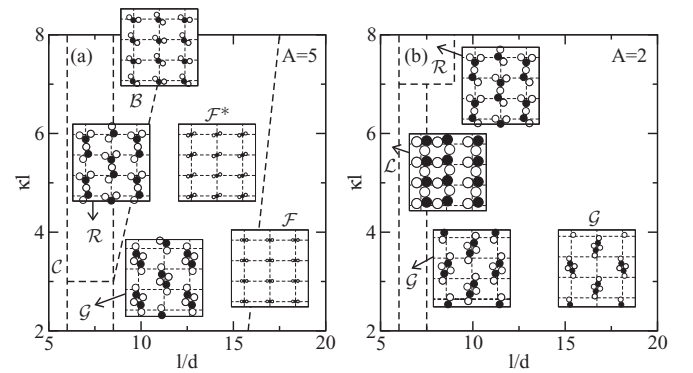


FIG. 8. Ground-state phase diagram for colloidal trimers on a rectangular lattice with $\alpha = 0.8$ and (a) $A = 5$ or (b) $A = 2$. Typical snapshot configurations in (a) are calculated using $(l/d, \kappa l) = (10, 8)$ for \mathcal{B} , $(7, 4)$ for \mathcal{R} , $(7, 2)$ for \mathcal{G} , $(15, 6)$ for \mathcal{F}^* , and $(20, 2)$ for \mathcal{F} phase; in (b) $(l/d, \kappa l) = (7, 8)$ for \mathcal{R} , $(5, 6)$ for \mathcal{L} , $(7, 2)$ for 2-partite \mathcal{G} , and $(10, 2)$ for 4-partite \mathcal{G} phase.

of complex subunits where each trimer touches three (out of four) neighboring trimers. Both pinning regimes involve also a distorted (or bent) rocket \mathcal{R} phase, which we identify as a variant of the existing ($\alpha = 1$) phase rather than a new phase itself, and a grape \mathcal{G} phase with 2- and 4-partite structures. Actually, in Fig. 8(b), almost the whole parameter space is minimized by a 4-partite grape \mathcal{G} configuration [27].

On a rectangular lattice, we can follow a similar line of reasoning as above in Sec. III A, where the occurrence of the \mathcal{A} phase was justified. In contrast to the situation on the square lattice, on the rectangular lattice the number of nearest-neighbor traps decreases to two, and to assess the stability of the \mathcal{F} phase, it is sufficient to consider a single triplet-triplet interaction of the form Eq. (4). In this case, the lowest energy configuration corresponds to parallel triplets ($\psi_1 = \psi_2 = 0$) forming a ferromagnetic-like arrangement along the longest direction of the lattice unit cell. This is indeed what is observed in Fig. 8(a) (see the \mathcal{F} region on the right-hand side), but not in Fig. 8(b), because in this latter case, confinement strength is too weak to prevent neighboring traps from sharing their macroions. We further note that the $\mathcal{F}^* \rightarrow \mathcal{B}$ transition visible in Fig. 8(a) falls in the same category as the $\mathcal{A} \rightarrow \mathcal{B}$ seen in Fig. 4: it is a one-cluster instability due to the competition between Coulomb and confinement forces. It is hence not surprising to find that the slopes of both separatrices are close: they are quantified by the same critical screening coefficient κ^* introduced above.

IV. TOWARD A MORE REALISTIC TRAP POTENTIAL

On a realistic trap, when allowing the particles to hop, we can expect to significantly extend the stability of the grapes, at least as soon as κd exceeds a small threshold. This is supported by the evaluation of the self-energies in Fig. 7, and we further analyzed the stability of the grape phase by explicitly introducing a cosine potential, which provides a reasonable approximation for a realistic optical confinement [7]:

$$V_T^{\text{real}} = -\frac{A_r}{2\pi^2} [\cos(2\pi x/l) + \cos(2\pi y/\alpha l)]. \quad (7)$$

The prefactor $2\pi^2$ is chosen such that both realistic and simplified potentials behave in the same way, as $(\delta/l)^2 = (x^2 + y^2)/l^2$ close to the trap minimum, when one chooses $A = A_r$.

In Figs. 9(b)–9(d), we show ground-state configurations for various pinning strengths A_r using the same parameter values $(l/d, \kappa l, \alpha)$ as in Fig. 9(a), where we show the four most representative parabolic-trap configurations. We choose A_r such that both potentials become similar in amplitude at the point of maximum V_T^{real} (see the left panel of Fig. 9). As A_r gets smaller [going from Fig. 9(b) to Fig. 9(d)], the optimal configurations indeed evolve to the grape \mathcal{G} geometry. In the limit $A_r \rightarrow A$, i.e., when the potentials share the same behavior close to the trap center, the lowest configurations are always grape \mathcal{G} phases. Although they have the same internal structure, these grapes are formed in realistic trap minima rather than at trap midpoints. In addition, the orientation of grapes is selected by the symmetry of the underlying realistic potential V_T^{real} , which is lowered with respect to the isotropic parabolic trap (the inset in the left panel of Fig. 9 shows the equipotential

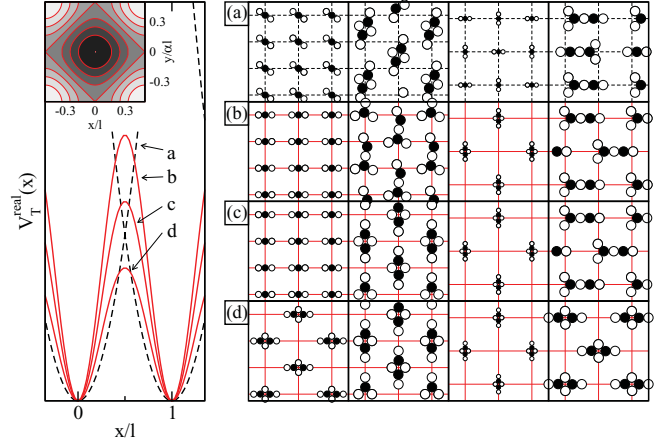


FIG. 9. (Color online) Comparison of structures calculated within an isotropic parabolic potential (a) and realistic cosine potential V_T^{real} (b)–(d) with three neighboring magnitudes A_r chosen to roughly correspond to the parabolic potential at the trap midpoint $x/l = 0.5$ (left panel). In (a) the parameter values are, from left to right, $(l/d, \kappa l, A, \alpha) = (10, 4, 5, 0.8)$ (\mathcal{F}^* phase), $(7, 2, 2, 0.8)$ (\mathcal{G} phase), $(15, 4, 5, 1)$ (\mathcal{A} phase), and $(7, 4, 2, 1)$ (\mathcal{R} phase). In (b)–(d) we use the same parameters as in (a) except V_T^{real} is used instead of parabolic trapping with $A_r = 20, 15, 10$ for $A = 5$ and $A_r = 8, 6, 4$ for $A = 2$.

lines of V_T^{real}). In fact, the realistic trap square symmetry is manifested in all configurations shown in Figs. 9(b)–9(d).

From Fig. 9, we see that switching to the realistic trap potential (V_T^{real}) preserves some typical cluster shapes (e.g., straight trimer, grape \mathcal{G} , rocket \mathcal{R}) from the parabolic case, while the positional or/and orientational order is generally altered. In a simple picture, the full consistency of both potentials (if any) would be found near the bottom of the trap where the realistic potential becomes isotropic, i.e., for $l/d \gg 1$. Since small A_r favor grape configurations that violate both the positional and orientational orders of the parabolic case, the consistency should be rather searched in the opposite limit of strong $A_r \gg 1$, where each trap should host exactly three colloids. In particular, the most promising phases are \mathcal{F} and \mathcal{A} phases since they also obey the symmetry constraints of V_T^{real} . To avoid bending of extended trimers in these two phases, we also anticipate small screening, i.e., $\kappa d \ll 1$, otherwise a banana \mathcal{B} shape might become more favorable.

Following these criteria and using a single-trap approximation (which is justified for small clusters), we identified regions in the $(\kappa l, l/d)$ parameter space (see the shaded areas in Fig. 10) where one straight trimer is energetically favorable against the banana \mathcal{B} and grape \mathcal{G} structures. In Fig. 10, we show such regions for realistic and parabolic potentials for a square and rectangular case (note that α has no effect in the parabolic approximation). The overlap between them gives an estimate where the consistency for \mathcal{F} (in $\alpha = 0.8$) and \mathcal{A} (in $\alpha = 1$) should be searched within a proper calculation including all neighboring traps. We have checked this at a few points of the phase diagram (symbols in Fig. 10) and indeed found consistency: the black circles in Fig. 10 denote the results where the all-neighbour calculation predicts the same phase [\mathcal{F} in Fig. 10(a) and \mathcal{A} in Fig. 10(b)] for both potentials. These results agree with the single trap prediction.

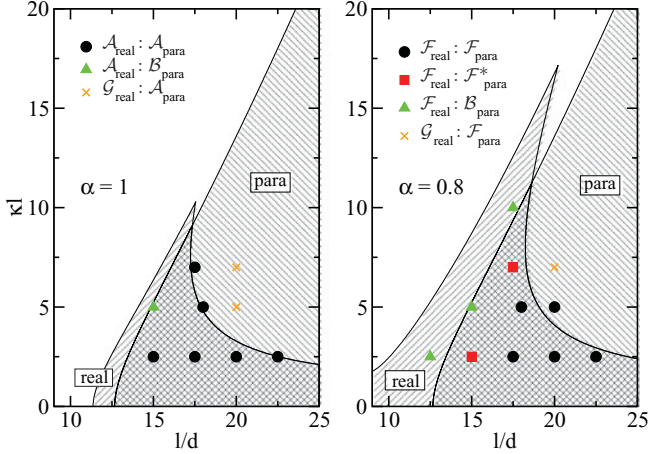


FIG. 10. (Color online) Single-trap calculations for parabolic (para) and realistic (real) trap potentials using $A = A_r = 50$ and $\alpha = 1$ (left panel) and $\alpha = 0.8$ (right panel). Shaded areas denote regions in parameter space where the straight trimer has lower energy than banana \mathcal{B} and grape \mathcal{G} clusters. The symbols are comparing full energy-minimization calculations for both trap potentials considering all neighboring traps: black disks denote exact consistency while the other symbols indicate that different phases are found with the “realistic” and parabolic confinement potentials.

To the left from the overlapping region (at smaller l/d), the inclusion of the neighboring traps introduces bending of the trimers and thus prefers the banana \mathcal{B} phase over the \mathcal{F} or \mathcal{A} (see the green triangles in Fig. 10). This effect is more visible for the parabolic potential since it is stronger than realistic when $A = A_r$. The above calculations were performed for a rather strong pinning strength ($A = A_r = 50$); however, we have checked and found \mathcal{F} and \mathcal{A} consistency also for weaker trap potentials, with $A = A_r \gtrsim 10$.

V. APPLYING AN EXTERNAL ELECTRIC FIELD

Since most of the observed phases are generally close in energy, it is tempting to explore how an external perturbation could change the phase behavior. We studied the response of

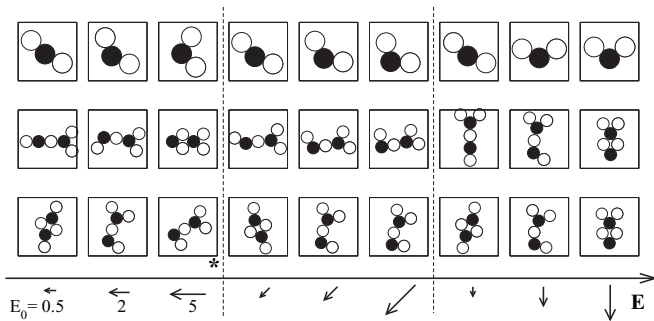


FIG. 11. Application of the external electric field \mathbf{E} on colloidal cluster shapes in the parabolic pinning regime for three field strengths E_0 and directions depicted at the bottom of the figure. The other parameters are $(l/d, \kappa l, A, \alpha) = (10, 4, 5, 0.8)$ in the first row, $(7, 4, 2, 1)$ in the second row, and $(7, 2, 2, 0.8)$ in the third row. The asterisk indicates that a cluster (when viewed periodically on a lattice) forms a percolated structure along the field direction.

the system to a static uniform electric field \mathbf{E} with the in-plane direction. Our primary purpose was to numerically investigate the possibility of external pattern switching [28] between the known phases, which might be appealing for experimental realizations. The ability to create and control colloidal crystal structures indeed has a wide range of applications in photonic and phononic materials, optical switches, photonic band-gap materials, and self-assembly of nanostructures [11].

In addition to either parabolic or cosine confinement, we use the following field potential at position (x, y) :

$$V_E = \pm E_0(x \cos \beta + y \sin \beta)/l, \quad (8)$$

where E_0 is a dimensionless field strength measuring the relative importance of external drag forces over Coulombic forces, and β is an angle between \mathbf{E} and the longest lattice principal axis. The “ \pm ” sign selects between positively and negatively charged colloids, respectively. The amplitude E_0 is considered small enough so that the system acquires an equilibrated ground-state configuration. This requirement is easily fulfilled in a parabolic trap approximation where, in principle, we never reach stationary regimes with drifting colloids [21] even for the largest values of E_0 . However, the opposite may happen in a realistic trap confinement [21] where at critical E_0 either cluster hopping or its breaking into smaller constituents takes place. We note that in the latter case, the critical field can be expressed analytically by $E_{c,2} = (1 + 2\kappa d) \exp(-2\kappa d)/(2d/l)^2$, above which the two oppositely charged colloids (a dimer) unbind. The breaking of a trimer occurs at slightly lower fields that can be estimated numerically by $E_{c,3} \sim 0.8E_{c,2}$.

We examined the influence of \mathbf{E} on the selected phases shown in Secs. III and IV using the EM and the gradient descent method. In Fig. 11, we show the results (one-trap snapshots) for parabolic trapping. Apart from rather trivial effects, such as bending (formation of the \mathcal{B} shape out of the straight trimer or a rocket \mathcal{R} deformation for $E_0 \leq 2$), we identified also more interesting effects at the strongest $E_0 = 5$: a new shape evolved from \mathcal{R} as well as \mathcal{G} structure, and an elongation of the modified \mathcal{G} complex along the field direction led to the formation of the percolated chain structure (denoted by an asterisk in Fig. 11).

In a similar manner, we demonstrate in Fig. 12 the influence of \mathbf{E} on a particular \mathcal{A} phase, again within a parabolic trap confinement; for $E_0 = 2$ and an electric-field angle $\beta = 0$ or $\pi/4$, we identify a pattern switching to a (quasi) \mathcal{F}^* phase. Here, the transition $\mathcal{A} \rightarrow \mathcal{F}^*$ appears to be on an orientational basis, with more or less minor shape deformations. Since the trimers of the field-induced \mathcal{F}^* phase are slightly shifted away from the trap center, the expected bending due to the electric field is (almost) compensated by the restoring trap forces, and the clusters appear almost straight.

We have also explored the effect of the external field within the real trap confinement. As found by Reichhardt *et al.* in Ref. [21], the colloids start to flow as soon as the electric-field force becomes larger than the real trap confinement, but here we focused instead on static configurations at smaller field strengths. In fact, in a large enough system, any constant electric field would inevitably lead to ground states with uneven population of the traps, i.e., the trimers would prefer

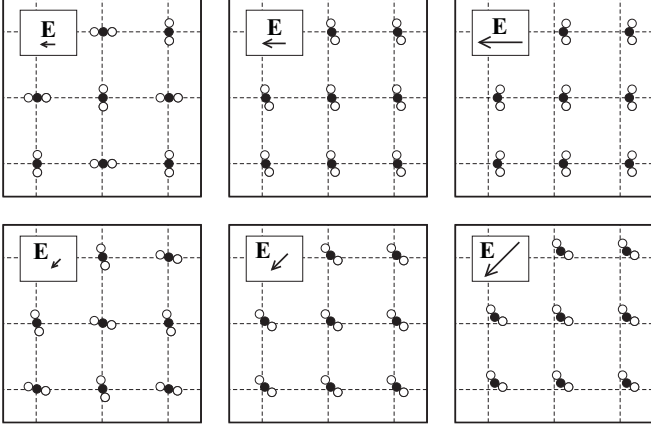


FIG. 12. Influence of an external electric field \mathbf{E} on the \mathcal{A} phase within the parabolic trap approximation for $(l/d, \kappa l, A, \alpha) = (15, 4, 5, 1)$. The field directions and magnitudes are shown with arrows in the inset of each plot; arrow lengths correspond to magnitudes $E_0 = 0.5, 2, 5$ of Eq. (8). For $E_0 = 2$ and $\beta = 0, \pi/4$ (the middle column), we observe a pattern switching to the \mathcal{F}^* phase (actually, its close approximation, since the trimers here are slightly bent with $\varphi_{1,2} \approx 0.91\pi$).

to move in the direction of the field to reduce the total energy of the system, leaving some of the traps at the opposite end empty. However, even though such states might have the lowest energy, they might not be accessible in the experiments and simulations. If, for instance, the system is first allowed to equilibrate at $\mathbf{E} = \mathbf{0}$ and then a small enough electric field is turned on, a local rather than global minimum is reached with colloids unable to surmount the large energy barriers on the way to the global minimum. This is the regime in which we are interested here.

To search for the nearest local energy minimum with an increasing electric field, we introduced a gradient descent method (i.e., a method of steepest descent) on a 4-partite lattice (16 model parameters; see Fig. 1) which brings a system continuously from an initial zero-field ground state to a finite-field metastable state using a finite step δE_0 (at fixed field direction β). Depending on the amplitude of the increment δE_0 , the switching of the field may be interpreted as fast or slow, something that can also be tuned in an experimental setup and may affect the outcome. In our calculations, we tried three step sizes, $\delta E_0 = 0.01, 0.1, 1$, and found basically no differences in the resulting configurations.

In Fig. 13, we show the evolution of \mathcal{A} and \mathcal{F} phases with increasing E_0 along two field directions using the highest field resolution $\delta E_0 = 0.01$. Focusing first on the \mathcal{A} phase (upper row in Fig. 13), we identify at $E_0 \approx 3$ (for both field directions) a rapid phase transition from a 2- to a 1-partite phase, which can also be viewed as a pattern switching to an approximate \mathcal{F}^* phase (with the internal angle being $\varphi \approx 0.8\pi$ rather than π), similar to what we found in the parabolic confinement (middle column in Fig. 12). This tendency of reducing the “partiteness” of the phase by increasing the external uniform field seems natural. However, the opposite situation is observed in the evolution of the \mathcal{F} phase, shown in Fig. 13(c), where in a short interval, $3 \lesssim E_0 \lesssim 4$, the metastable phase adopts a higher, 2-partite \mathcal{B} structure. This rather surprising effect reflects the

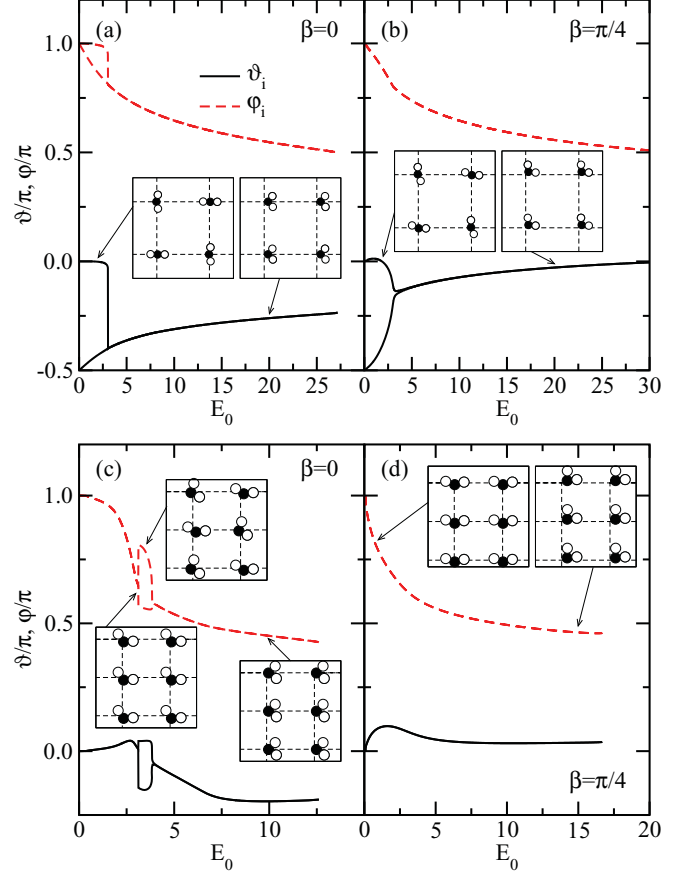


FIG. 13. (Color online) Local energy minima configurations represented by trimer angles ϑ_i (solid line) and φ_i (dashed) as a function of external electric field E_0 using the cosine confinement potential Eq. (7). The index $i = 1, \dots, 4$ represents the four different values for a 4-partite lattice assumption. The upper row is calculated from initial ($E_0 = 0$) \mathcal{A} phase with $(l/d, \kappa l, A_r/(2\pi^2), \alpha) = (15, 4, 1.5, 1)$ for two field directions (a) $\beta = 0$ and (b) $\beta = \pi/4$. In the lower row, the initial ($E_0 = 0$) state is the \mathcal{F} phase with $(l/d, \kappa l, A_r/(2\pi^2), \alpha) = (10, 4, 0.75, 0.8)$ and field directions are again (c) $\beta = 0$ and (d) $\beta = \pi/4$. In all the plots, we used a field resolution $\delta E_0 = 0.01$. A few representative snapshots are added for illustration (see the supplemental material [29] for the animated cartoons).

richness of the system studied, where the observed phases differ only slightly in energy and can therefore interchange easily under external perturbation. At larger field strengths again a uniform pattern takes place [28].

We note that a similar field-evolution study in cosine trap confinement was done also for two representative \mathcal{G} and \mathcal{R} phases with six colloids per trap, but we found no striking effects apart from trivial bending of the clusters, which was already observed in a parabolic confinement (see, e.g., Fig. 11). These results are included in the form of animated cartoons available in the online supplemental material [29].

VI. CONCLUSION

In summary, we have studied ordering of colloidal ionic trimers on square lattices. We observed a rich variety of crystal structures, including crystals made of complex six-colloid subunits. We have discussed their stability and the possibility

for pattern switching by external control, which might be appealing for experimental realizations and applications.

In the case of the isotropic confinement potential, the symmetry is broken by the Yukawa interactions only. The orientational ordering is of an “intrinsic nature” and does not stem from an anisotropy present in the confinement potential itself. Three colloids can form a straight line or a bent banana-shaped trimer. We have identified the parameter range where both are stable and the types of their orientational ordering. In the low κ and small l/d part of the phase diagrams, where the intercluster interactions typically outweigh the confinement, the neighboring trimers cluster into larger complexes consisting of six colloids, their typical shapes being grape and rocket. At even smaller l/d and κ , the colloids form percolated structures. Here, however, many-body effects [30] are expected to become significant and our assumption of the pairwise additivity of the colloid-colloid interaction becomes questionable [31,32]. We have shown that most of the phases observed in the isotropic confinement persist also in the more realistic anisotropic external potential, provided that the confinement strength is large enough. However, their orientational ordering in the latter case is different due to the additional symmetry breaking by the laser field. The rich selection of the ground-state structures and the relatively small energy differences between them enable efficient control over

the structures by applying external fields. We have analyzed the effect of a small external electric field and have shown that it can be used as a pattern-switching tool.

Not addressed here, but a subject for future work, is the thermal behavior of the system. Another unresolved question is the effect of the interaction potential on the stability of the observed structures, and in the many-body interactions among colloids that are expected to be important at high densities. Finally, in addition to systems with oppositely charged colloids, externally driven superparamagnetic colloids [33] and colloids interacting via Casimir interaction in critical binary mixtures [34] may offer instances in which the present predictions—or adaptations thereof—could be realized.

ACKNOWLEDGMENTS

We acknowledge the support of the bilateral program Proteus of the Slovenian Research Agency and the French Ministère des Affaires Étrangères et Européennes, the support of the Slovenian research agency through Grant No. P1-0055, and the support of the EU through the ARG (ERC-COLSTRUCTION 227758) and the 7th Framework Programme (ITN-COMPLOIDS 234810). J.D. would like to acknowledge the hospitality of Aspen Center for Physics.

-
- [1] E. S. Hedges, *Colloids* (Hedges, 2007). This monograph dates back to 1931 and offers an instructive overview of the state of the art at that time.
- [2] B. V. Derjaguin and L. Landau, *Acta Physicochim USSR* **14**, 633 (1941); E. J. W. Verwey and J. T. G. Overbeek, *Theory of the Stability of Lyophobic Colloids* (Dover, Amsterdam, 1997).
- [3] See, e.g., D. Frenkel, *Introduction to Colloidal Systems*, in *Soft Condensed Matter Physics in Molecular and Cell Biology*, edited by W. C. K. Poon and D. Andelman (Taylor and Francis, New York, London, 2006).
- [4] W. C. K. Poon, *Science* **304**, 830 (2004).
- [5] M. E. Leunissen, C. G. Christova, A. P. Hynninen, C. P. Royall, A. I. Campbell, A. Imhof, M. Dijkstra, R. van Roij, and A. van Blaaderen, *Nature (London)* **437**, 235 (2005).
- [6] M. Brunner and C. Bechinger, *Phys. Rev. Lett.* **88**, 248302 (2002).
- [7] C. Reichhardt and C. J. Olson-Reichhardt, *Phys. Rev. Lett.* **88**, 248301 (2002); C. J. Olson-Reichhardt and C. Reichhardt, *J. Phys. A* **36**, 5841 (2003); C. Reichhardt and C. J. Olson-Reichhardt, *Phys. Rev. E* **71**, 062403 (2005).
- [8] R. Agra, F. van Wijland, and E. Trizac, *Phys. Rev. Lett.* **93**, 018304 (2004).
- [9] A. Sarlah, T. Franosch, and E. Frey, *Phys. Rev. Lett.* **95**, 088302 (2005); A. Sarlah, E. Frey, and T. Franosch, *Phys. Rev. E* **75**, 021402 (2007).
- [10] S. El Shawish, J. Dobnikar, and E. Trizac, *Soft Matter* **4**, 1491 (2008).
- [11] K. Mangold, P. Leiderer, and C. Bechinger, *Phys. Rev. Lett.* **90**, 158302 (2003); J.-X. Lin, C. Reichhardt, Z. Nussinov, L. P. Pryadko, and C. J. Olson-Reichhardt, *Phys. Rev. E* **73**, 061401 (2006); J. Baumgartl, M. Zvyagolskaya, and C. Bechinger, *Phys. Rev. Lett.* **99**, 205503 (2007); D. Deb and H. H. von Grunberg, *J. Phys. Condens. Matter* **20**, 245104 (2008); M. Schmiedeberg and H. Stark, *Phys. Rev. Lett.* **101**, 218302 (2008).
- [12] E. Trizac, S. El Shawish and J. Dobnikar, *An. Acad. Bras. Ciênc* **82**, 87 (2010).
- [13] As will be discussed later, our model differs in some aspects from the one considered in Ref. [9], where only discrete orientations were considered for the colloidal n -mers. Within such a framework, some approximations, backed up by Monte Carlo simulations, have been put forward to unravel the effect of temperature [9].
- [14] M. Brunner and C. Bechinger, *Prog. Colloid Polym. Sci.* **123**, 156 (2004).
- [15] J.-P. Hansen and H. Löwen, *Annu. Rev. Phys. Chem.* **51**, 209 (2000).
- [16] Y. Levin, *Rep. Prog. Phys.* **65**, 1577 (2002).
- [17] E. Trizac, L. Bocquet, and M. Aubouy, *Phys. Rev. Lett.* **89**, 248301 (2002).
- [18] L. Belloni, *Colloids Surf. A* **140**, 227 (1998); *J. Phys. Condens. Matter* **12**, R549 (2000).
- [19] It is worth stressing that the ground states we consider here are reached at constant κ while the latter is a temperature-dependent quantity. Such a point of view—consistent with the numerical approach of [7]—requires considering large pinning amplitudes (strong laser fields) at constant temperature and constant electrolyte density from an experimental perspective. However, compared to the like-charge colloidal cases studied previously [6–11], there is no need here to tune correlatively the colloidal charge, since within a composite molecule in a given trap, the colloids are in contact: in the like-charge case, the

- extension of the molecules depends critically on the confinement amplitude, whereas here, this amplitude only affects the shape of the molecules, but not their extension.
- [20] J. Groenewold and W. Kegel, *J. Phys. Chem. B* **105**, 11702 (2001); A. Stradner, H. Sedgwick, F. Cardinaux, W. C. Poon, S. U. Egelhaaf, and P. Schurtenberger, *Nature (London)* **432**, 492 (2004); A. I. Campbell, V. J. Anderson, J. S. van Duijneveldt, and P. Bartlett, *Phys. Rev. Lett.* **94**, 208301 (2005); S. Mossa, F. Sciortino, P. Tartaglia, and E. Zaccarelli, *Langmuir* **20**, 10756 (2004); S. Jiang, Q. Chen, M. Tripathy, E. Luitjen, K. S. Schweizer, and S. Granick, *Adv. Mater.* **22**, 1060 (2010).
- [21] C. Reichhardt and C. J. Olson-Reichhardt, *Phys. Rev. E* **79**, 061403 (2009).
- [22] See, e.g., *Numerical Recipes, The Art of Scientific Computing* (Cambridge University Press, New York, 1992).
- [23] We stress that our system exhibits at least two energy scales: the larger one is defined by the attractive Coulomb interaction between two touching colloids and is of the order $1/2d$, while the smaller one is the Yukawa interaction between the traps of the order $\exp(-\kappa l)/l$ and is responsible for orientational order. The $4p$ -dimensional energy surface is therefore composed of deep minima each of which has again many shallow minima.
- [24] This mechanism somehow resembles the strain-induced colloidal clustering on periodic (triangular) substrates with more traps than colloids [35]. Another somewhat related phenomenon is the appearance of the so-called cluster crystals in systems with soft repulsive potentials [36–39], although the present system is more complex and a delicate interplay between the external confinement and the colloidal interactions governs its behavior.
- [25] E. Trizac, L. Bocquet, R. Agra, J.-J. Weis, and M. Aubouy, *J. Phys. Condens. Matter* **14**, 9339 (2002).
- [26] R. Agra, E. Trizac, and L. Bocquet, *Eur. Phys. J. E* **15**, 345 (2004).
- [27] At smaller l/d , the checkerboard structure eventually becomes less favorable against a 2-partite structure: the corresponding energies, for instance, change from $E_{4p}/K = -1.718$, $E_{2p}/K = -1.717$ for $(l/d, \kappa l) = (10, 2)$ to $E_{4p}/K = -0.9199$, $E_{2p}/K = -0.9203$ for $(l/d, \kappa l) = (7, 2)$.
- [28] C. Reichhardt and C. J. Olson Reichhardt, *Phys. Rev. E* **80**, 022401 (2009).
- [29] See supplemental material at [<http://link.aps.org/supplemental/10.1103/PhysRevE.83.041403>] for animated images showing various local minimum configurations.
- [30] M. Brunner, J. Dobnikar, H. H. von Grünberg, and C. Bechinger, *Phys. Rev. Lett.* **92**, 078301 (2004); J. Dobnikar, M. Brunner, H. H. von Grünberg, and C. Bechinger, *Phys. Rev. E* **69**, 031402 (2004).
- [31] J. Dobnikar, Y. Chen, R. Rzehak, and H. H. von Grünberg, *J. Chem. Phys.* **119**, 4971 (2003).
- [32] D. Reinke, H. Stark, H. H. von Grünberg, A. B. Schofield, G. Maret, and U. Gasser, *Phys. Rev. Lett.* **98**, 038301 (2007).
- [33] N. Osterman, I. Poberaj, J. Dobnikar, D. Frenkel, P. Ziherl, and D. Babič, *Phys. Rev. Lett.* **103**, 228301 (2009).
- [34] C. Hertlein, L. Helden, A. Gambassi, S. Dietrich, and C. Bechinger, *Nature (London)* **451**, 172 (2008); F. Soyka, O. Zvyagolskaya, C. Hertlein, L. Helden, and C. Bechinger, *Phys. Rev. Lett.* **101**, 208301 (2008).
- [35] S. Bleil, H. H. von Grünberg, J. Dobnikar, R. Castaneda Priego, and C. Bechinger, *Europhys. Lett.* **73**, 450 (2006).
- [36] B. M. Mladek, P. Charbonneau, and D. Frenkel, *Phys. Rev. Lett.* **99**, 235702 (2007).
- [37] S. van Teeffelen, A. J. Moreno, and C. N. Likos, *Soft Matter* **5**, 1024 (2009).
- [38] N. Osterman, D. Babič, I. Poberaj, J. Dobnikar, and P. Ziherl, *Phys. Rev. Lett.* **99**, 248301 (2007).
- [39] J. Dobnikar, J. Fornleitner, and G. Kahl, *J. Phys. Condens. Matter* **20**, 494220 (2008).